Electronic Supplementary Material (ESI) for Journal of Materials Chemistry A.

[Electronic Supplementary Information]

Maghemite nanoparticles decorated on carbon nanotubes as an efficient electrocatalyst for oxygen evolution reaction

Mohammad Tavakkoli,[*a] Tanja Kallio,[a] Olivier Reynaud,[b] Albert G. Nasibulin,[bcd] Jani Sainio,[b] Hua Jiang,[b] Esko I. Kauppinen[b] and Kari Laasonen [*a]

[a] *Department of Chemistry, Aalto University, School of Chemical Technology, P.O. Box 16100, FI-00076 Aalto, Finland. Email: mohammad.tavakkoli@aalto.fi, kari.laasonen@aalto.fi*

[b] *Department of Applied Physics, Aalto University, School of Science, P.O. Box 15100, FI 00076 Aalto, Finland*

[c] *St. Petersburg Polytechnic University, 195251, St. Petersburg, Russia*

[d] *Skolkovo Institute of Science and Technology, 143025, Skolkovo, Moscow Region, Russia*

Experimental section

Synthesis of CEIN/CNT: Carbon-encapsulated iron nanoparticles (CEINs) decorated on carbon nanotubes (CNTs) were grown in a gas phase reaction with an aerosol chemical vapor deposition (CVD) technique. The reactants were introduced in a 5 cm diameter quartz tube heated at a synthesis temperature of 1100 ˚C by a furnace with 60 cm long hot zone. A liquid feedstock containing ferrocene ($C_{10}H_{10}Fe$) and thiophene (C_4H_4S) dissolved in toluene (C_7H_8) was introduced with a mass flow of 5 g/h and atomized by a nitrogen jet flow. The liquid feedstock solution was prepared with 4% wt. of ferrocene in toluene, and thiophene was added to the solution so that the molar concentration of ferrocene and thiophene are both equal to 0.186 mol/L. Thiophene was utilized as a promoter for the growth of CNTs. The aerosol of feedstock solution was carried into the reactor by an 8 lpm hydrogen (H_2) flow. Carbon used for the CEIN/CNT synthesis was provided by the catalytic decomposition of toluene and ethylene (C_2H_4). Ethylene was introduced into the reactor at a flow rate of 17 cm^3/min. The growth of the CNTs occurred on iron catalyst particles formed in the gas phase by the thermal decomposition of ferrocene. The synthesis took place in atmospheric pressure and in laminar flow conditions inside the reactor. The CEIN/CNT sample was filtered from the gas phase at the outlet of the reactor with a nitrocellulose membrane filter (Millipore, 0.45 µm diameter pores). A scheme of the synthesis reactor is shown in Figure S1.

Characterization:

Electron microscopy: For TEM characterizations, the CEIN/CNT material was dispersed in ethanol (0.02 mg/ml) and then 2 µl of the solution was drop cast on a carbon coated TEM grid and dried in ambient air. The product was observed through a JEOL-2200FS, double Cs-corrected HRTEM at the acceleration voltage of 200 kV.

Raman Analysis: The Raman spectrum (632.8 nm, JY LabRam 300) of CEIN/CNT is shown in Figure S5. The radial breathing modes (RBM) appearing at Raman shifts of 100 – 350 cm^{-1} result from the symmetric movement of carbon atoms in the radial direction and only appear for single-walled or double-walled CNTs. Here, only a few weak RBM peaks appear for the CEIN/CNT sample, representing a very low amount of single-walled or double-walled CNTs which is in agreement with HRTEM images as most of the observed CNTs are few-walled CNTs. G band at 1589 cm^{-1} and D band at 1320 cm^{-1} are observed and correspond to the vibration of carbon atoms in a graphite layer and the presence of defects in the nanotubes or amorphous carbon materials, respectively.[1]

XPS Analysis: X-ray photoelectron spectroscopy (XPS) from the catalyst material was done using a Surface Science Instruments SSX-100 ESCA spectrometer with monochromated Al K_α radiation. Full-range and C1s XPS spectra of the CEIN/CNT material before and after 3 anodic sweeps (potential sweep between 1 - 1.65 V vs RHE) in 1 M NaOH, which changes the material mostly to g-Fe_2O_3/CNT, are shown in Figure S6. In figure S6b showing C 1s XPS spectra of the CEIN/CNT and g-Fe_2O_3/CNT samples, there are a clear main peak at around 284.5 eV and shoulder peaks at higher binding energies (between 285 and 288 eV) which are attributed to C-C bonds of the CNTs and various oxygen related bonds (C-O, C=O, O-C=O), respectively.[2] After the anodic sweeps, there is a small increase of the relative intensity of the shoulder peak region in the C 1s spectrum which can be attributed to the presence of oxygen-containing groups on the CNTs surface. The shake-up satellite peak at 290.6 eV is attributed to a π-π * transition.[3]

Electrochemical Procedures

The electrochemical measurements were carried out using a three-electrode cell. Linear sweep voltammetry with a 5 mV s^{-1} scan rate was performed in 0.1 M and 1 M NaOH electrolyte solutions. The reference, counter, and working electrodes were a reversible hydrogen electrode (RHE), a platinum wire, and a glassy carbon electrode, respectively. Pristine SWNTs (with diameter distribution of 0.8-1.2 nm, purchased from Unidym), platinum on carbon black (Pt/C purchased from Alfa Aesar), and IrO_2 (purchased from Sigma Aldrich) were used for comparison with the CEIN/CNT sample. The catalyst materials (SWNTs, Pt/C, and IrO_2) were dispersed in ethanol and then stirred (for 30 min) and sonicated (for 30 min) to form homogeneous inks. The inks were then deposited on glassy carbon electrodes with a loading of ~0.2 mg cm^{-2} and dried in air. Subsequently, 25 µl of 5 wt% Nafion was diluted with 1 ml of ethanol; 5 µl of that solution was then added on top of the catalyst layers as binder. Prior to any measurements, all the electrodes were cycled 50 cycles between -0.05 and 1.15 V versus RHE at 50 mV s^{-1} scan rate in nitrogen protected electrolyte solution. For the choronoamperometry measurements, instead of glassy carbon, graphitized carbon fiber paper (CFP) was utilized as the electrode substrate since the adhesion of CNTs on the CFP electrode is higher that than that on glassy carbon.

Unless specifically mentioned, rotating disc electrode (RDE) voltammograms were depicted without iR compensation. The uncompensated ohmic electrolyte resistance (R_u) was determined by equating R_u to the minimum total impedance in a non-Faradaic region measured between 10 Hz and 100 kHz, where the capacitive and inductive impedances are negligible and the phase angle was near zero. The values of R_u ~ 20 Ω and R_u ~ 4 Ω were recorded in 0.1 and 1 M NaOH solutions respectively.

Calculation of electrochemically active surface area

The electrochemical capacitance was calculated by measuring double layer capacitance of g-Fe_2O_3/CNT on a glassy carbon RDE in 1 M NaOH in a similar way to what previously published.[4,5] To measure double layer capacitance, the cyclic voltammograms (CVs) at different scan rates in a potential range where no Faradaic process occurred were plotted (Figure S8a) and charging currents (i_c) at different scan rates were measured. From the slope of i_c as a function of scan rate (u), the double layer capacitance (C_{DL}) was obtained (Figure S8b) based on the following eq 1:

$$i_c = uC_{DL} \quad (1)$$

The C_{DL} of g-Fe_2O_3/CNT measured by the above-mentioned method is ~ 1.4 mF.

The electrochemically active surface area (ECAS) can be obtained from eq 2:

$$ECAS = C_{DL}/C_s \quad (2)$$

Where C_s is specific capacitance. The average C_s of 0.040 mF cm^{-2} in 1 M NaOH was used in the calculation of the ECAS based on previous reports[4,5] in alkaline solution. As a result, an ECAS of 35 cm^2 was obtained for the g-Fe_2O_3/CNT catalyst.

The geometric surface area (GSA) of the catalyst material deposited on the glassy carbon RDE was 0.125 cm^2, therefore the roughness factor (RF) of 280 was obtained from eq 3:

$$RF = ECAS/GSA \quad (4)$$

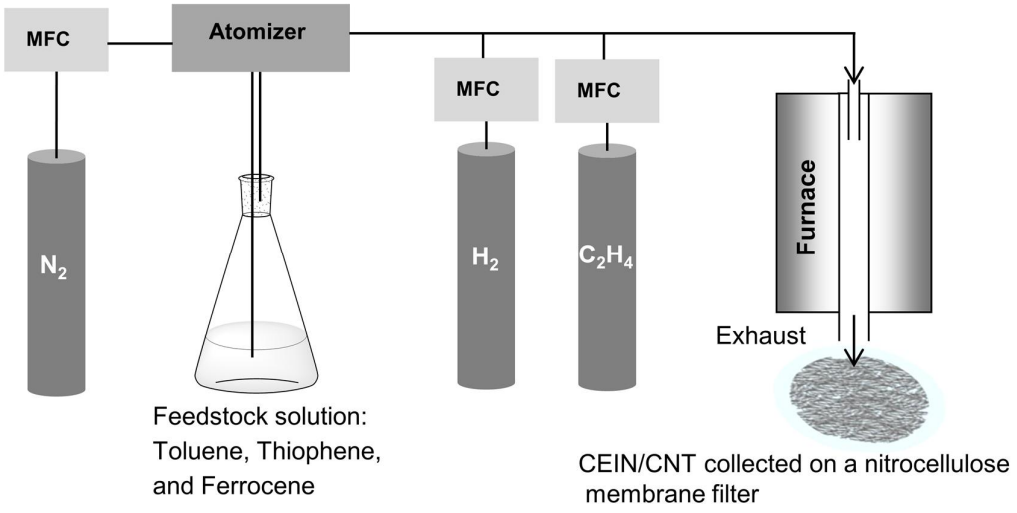

Figure S1. A scheme of the synthesis reactor used for the growth of CEIN/CNT (MFC is referred to mass flow controller).

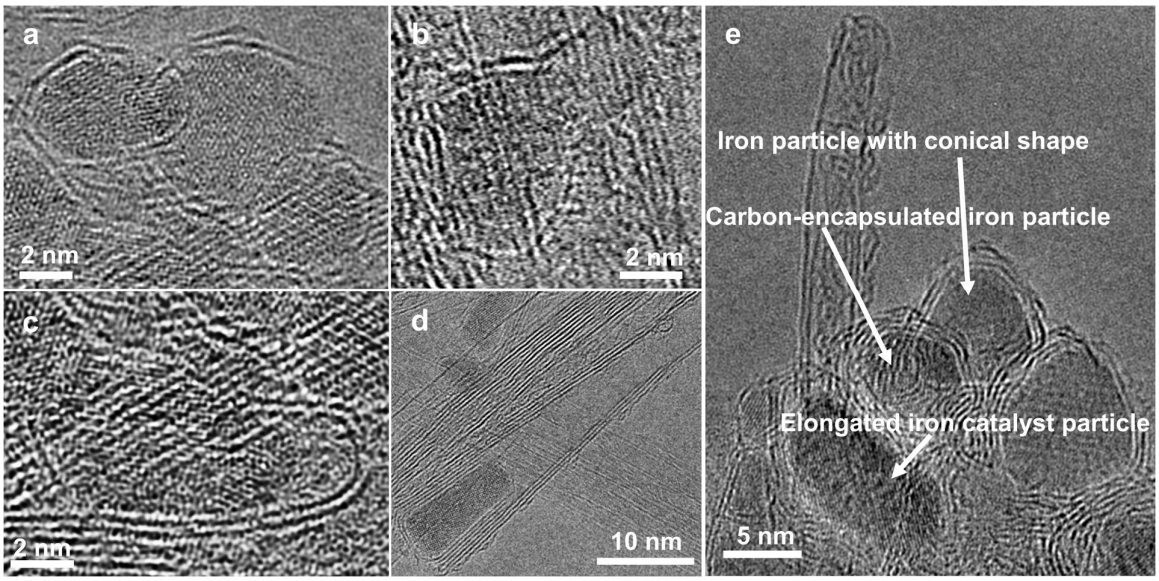

Figure S2. ***HRTEM images of CEIN/CNT representing iron nanoparticles at different stages of the growth of CNTs.*** **a,** Carbon encapsulated iron nanoparticles; **b** and **c,** Iron nanoparticles with a conical shape and the formation of the carbon cap; **d,** Elongated iron particle surrounded by a CNT; **e,** The presence of all types of the shown iron particles with different structures in images a-d, in the CEIN/CNT sample.

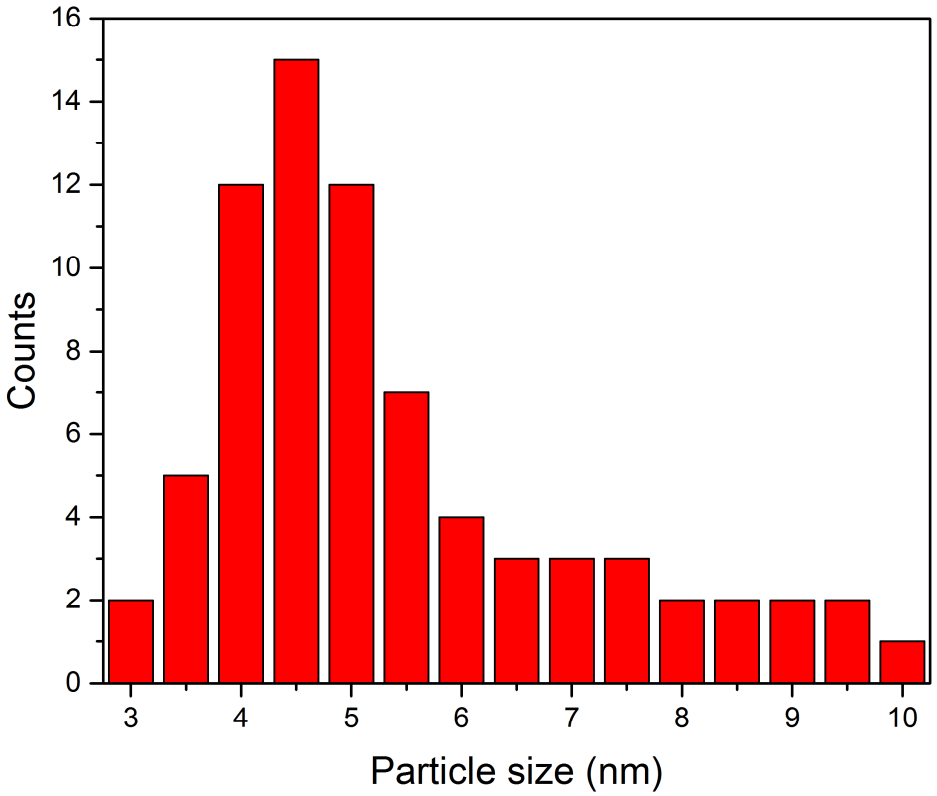

Figure S3. Particle size distribution of the iron nanoparticles in CEINs. Size distribution analysis of the iron nanoparticles in CEINs was performed by measuring 75 individual nanoparticles from the HRTEM images. Less than 5% of the iron particle sizes in CEINs were out of the size distribution shown in this figure.

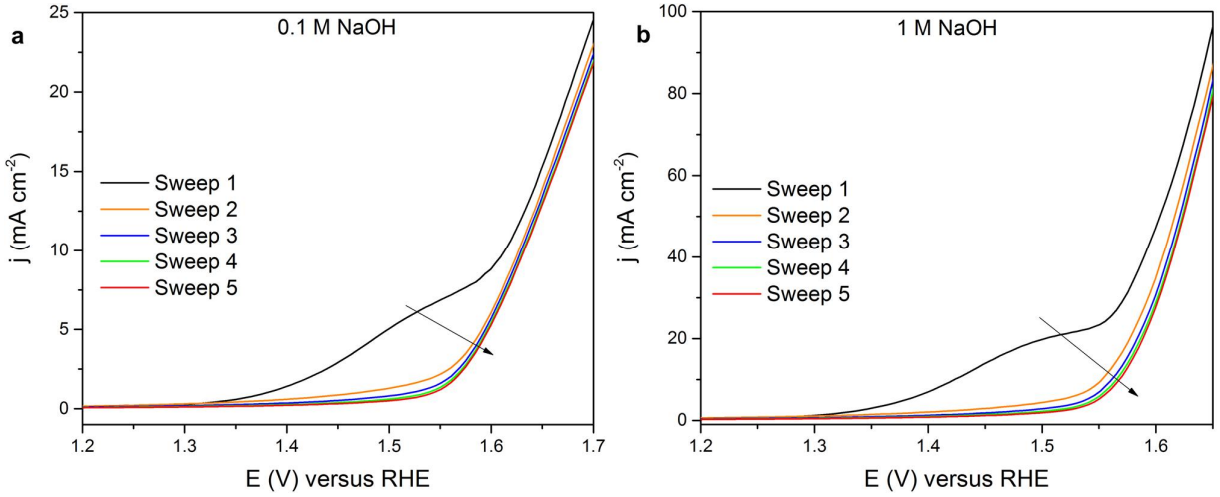

Figure S4. The first five OER anodic potential sweeps for the CEIN/CNT sample measured at a scan rate of 5 mV s^{-1} and a rotation of 1600 r.p.m in **a,** 0.1 and **b,** 1 M NaOH alkaline solutions without iR compensation.

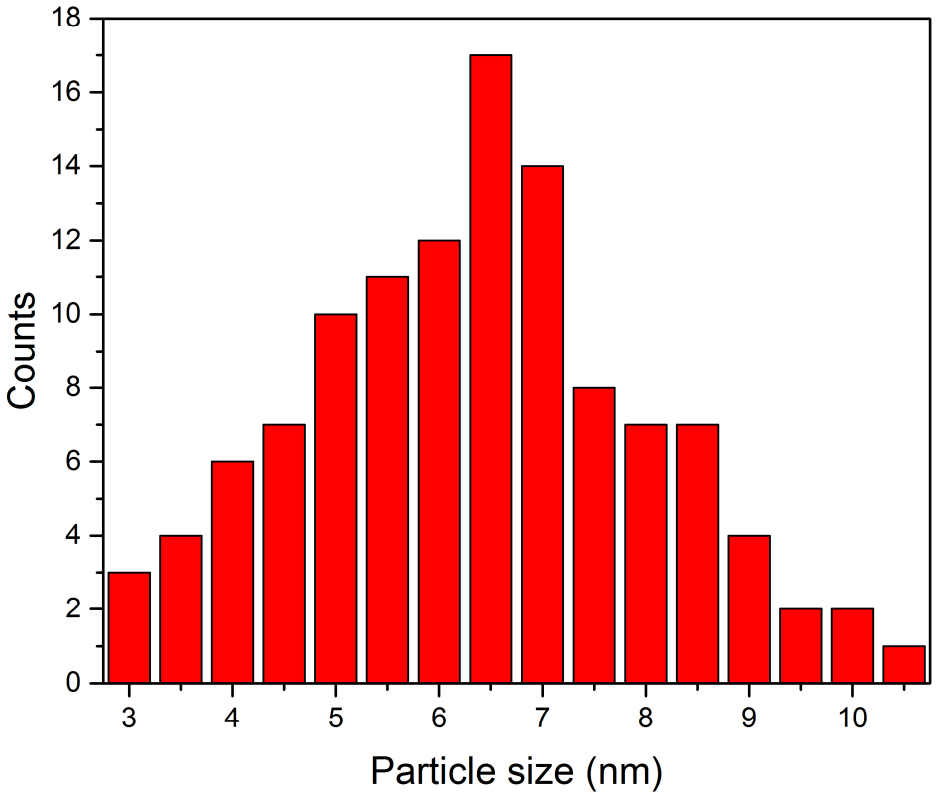

Figure S5. Particle size distribution of the g-Fe_2O_3 nanoparticles. Size distribution analysis of the nanoparticles was performed by measuring 115 individual nanoparticles from the HRTEM images.

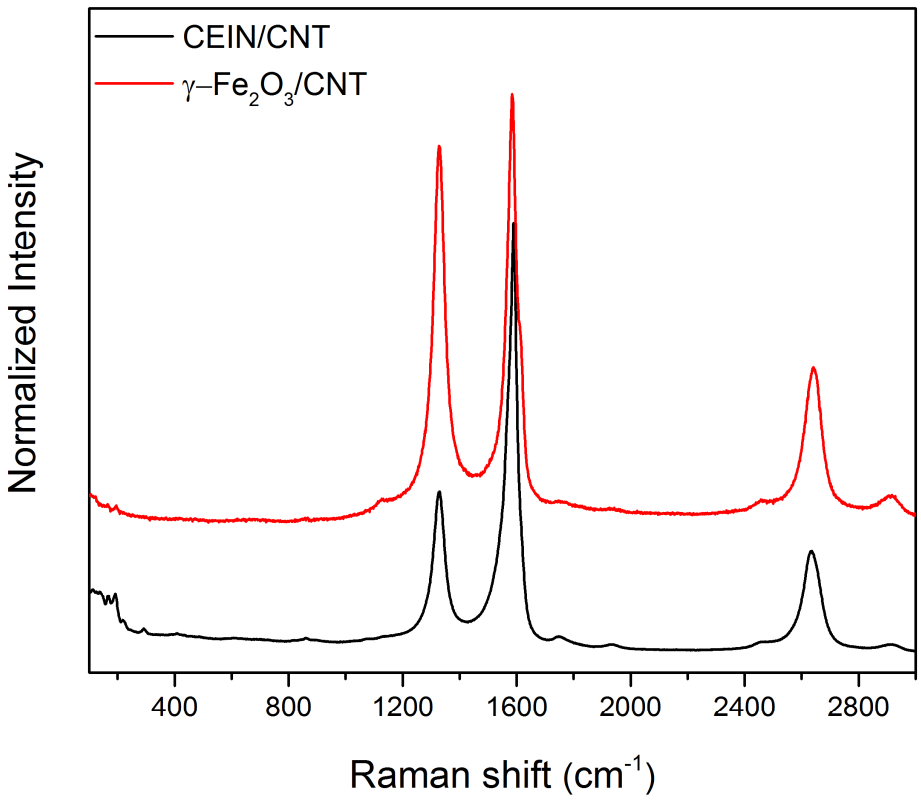

Figure S6. Raman spectra of the CEIN/CNT (black line) and g-Fe_2O_3/CNT (red line) samples. All spectra are normalized with respect to their respective G band intensities.

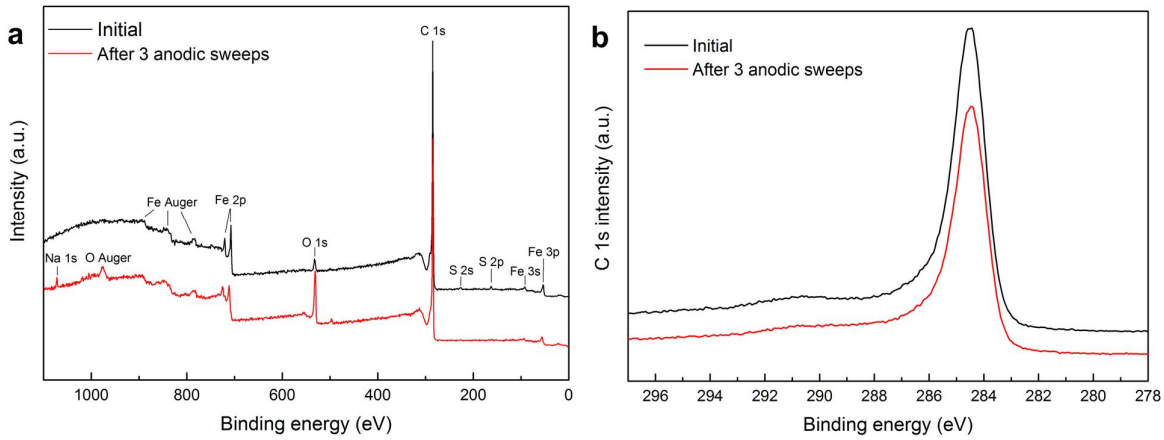

Figure S7. a, Full-range and **b,** C 1s XPS spectra of the CEIN/CNT material before (black lines) and after (red lines) 3 anodic potential sweeps (potential sweep between 1 - 1.65 V vs RHE) at a scan rate of 5 mV s^{-1} and a rotation of 1600 r.p.m in 1 M NaOH.

Table S1. The atomic and weight percentages of the elements in the CEIN/CNT sample before and after 3 anodic potential sweeps (potential sweep between 1 - 1.65 V vs RHE) at a scan rate of 5 mV s^{-1} and a rotation of 1600 r.p.m in 1 M NaOH. The presence of Na in the sample after 3 sweeps originates from the residual Na from the electrolyte.

Element	CEIN/CNT		CEIN/CNT after 3 OER sweeps in 1 M NaOH	
	Atomic %	Weight %	Atomic %	Weight %
C	94	83.7	82.9	69.3
O	2.4	2.9	12.1	13.5
Fe	2.8	11.5	4	15.4
S	0.8	1.9	0.3	0.8
Na	0	0	0.7	1

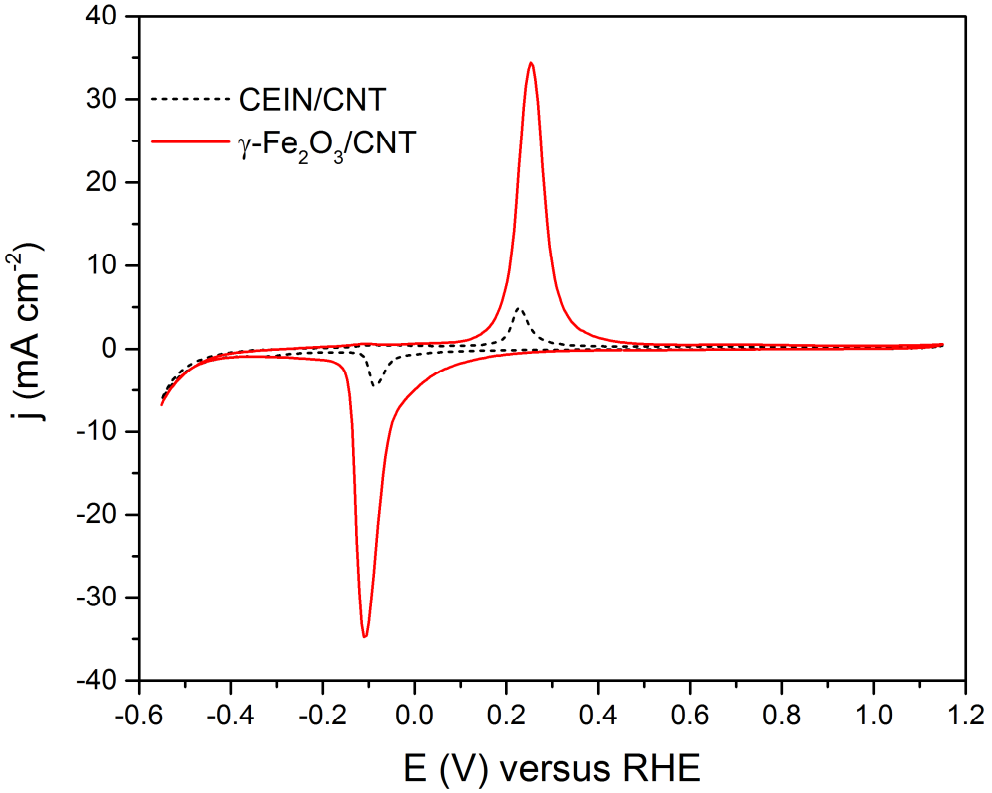

Figure S8. Cyclic voltammetry (CV) curves of CEIN/CNT (black dash line) and CEIN/CNT after OER current stabilization (g-Fe_2O_3/CNT, red solid line) in 1 M NaOH. The CVs were measured at a scan rate of 20 mV s^{-1} in N_2-saturated 1 M NaOH alkaline solution.

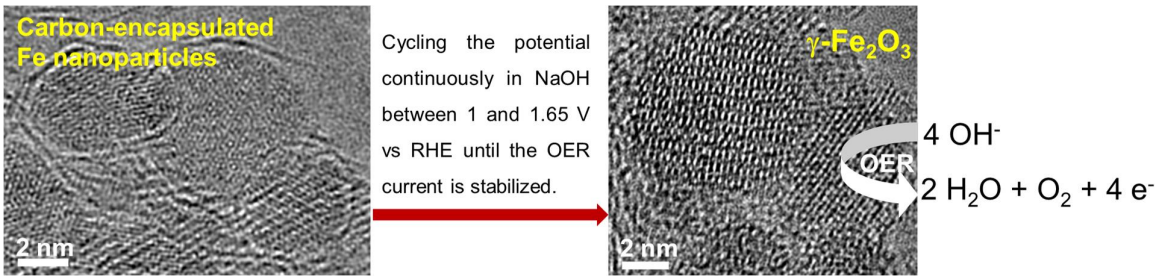

Figure S9. Representation of replacing CEINs with g-Fe_2O_3 nanoparticles via cycling the potential of CEIN/CNT coated glassy carbon electrode between 1 and 1.65 V vs RHE in the alkaline NaOH solution.

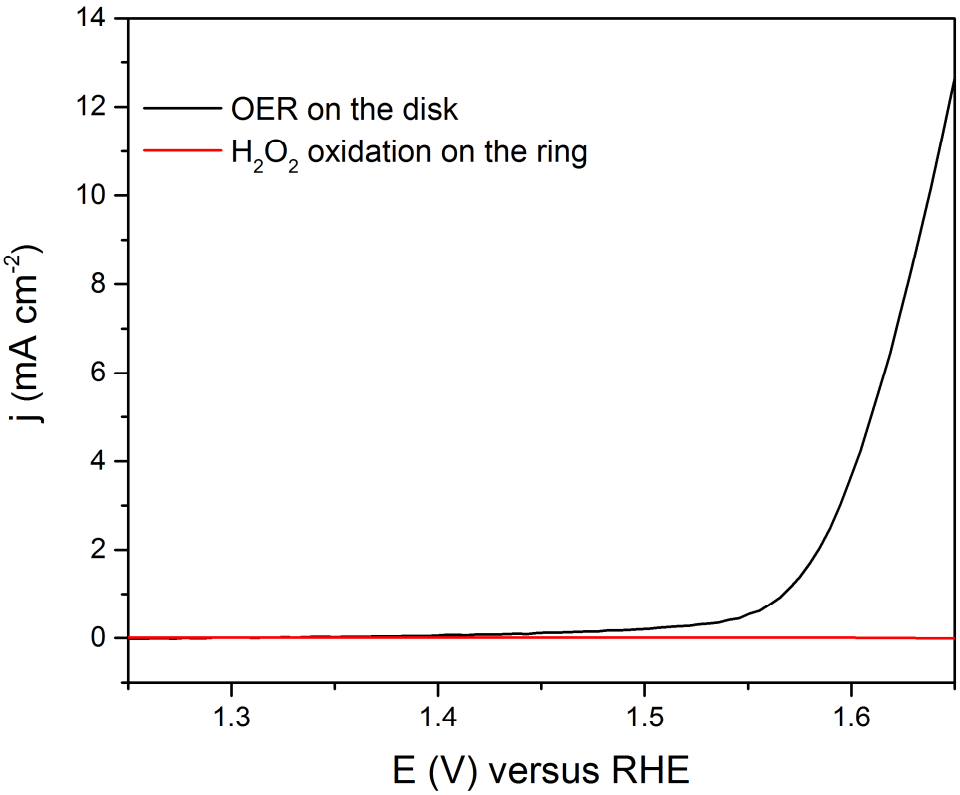

Figure S10. Detection of H_2O_2 generated from the g-Fe_2O_3/CNT catalyst using RRDE measurements. The ring potential was kept at 1.4 V for monitoring H_2O_2 production at the disc electrode during the OER sweep. The polarization curves were measured at a scan rate of 5 mV s^{-1} and a rotation of 1600 r.p.m in the alkaline 0.1 M NaOH solution.

Table S2. Comparison of the OER activity in alkaline conditions for g-Fe_2O_3/CNT with several recently reported highly active transition-/noble-metal and non-metal catalysts supported on glassy carbon electrode.

Catalyst	Electrolyte	Potential at 10 mA cm^{-2} (V vs RHE)	Tafel slope (mV/dec)	Mass loading (mg cm^{-2})	Reference
g-Fe_2O_3 nanoparticles/CNT	0.1 M NaOH	1.61	50	0.2	This work
	1 M NaOH	1.57	45		
IrO_2/C	0.1 M KOH	1.6	N.A.	0.2	6
N-Co_9S_8/graphene	0.1 M KOH	1.639	82.7	0.2	7
N-doped graphene-CoO	1 M KOH	1.57	71	0.7	8
g-C_3N_4-CNT composite	0.1 M KOH	1.6	83	0.2	9
N-doped graphitic carbon	0.1 M KOH	1.61	75-80	0.2	6
Mn_3O_4/$CoSe_2$ nanocomposite	0.1 M KOH	1.68	49	0.2	10
IrO_x	1 M NaOH	1.55	N.A.	N.A.	4
$NiFeO_x$ $CoFeO_x$ $NiCoO_x$ CoO_x $NiLaO_x$ $NiCuO_x$ CoOx/CoPi NiO_x $NiCeO_x$	1 M NaOH	1.59 ↓ 1.66	N.A.	N.A.	4
echo-MWCNTs	0.1 M KOH	1.68	72	0.2	5
	1 M KOH	1.59	41		

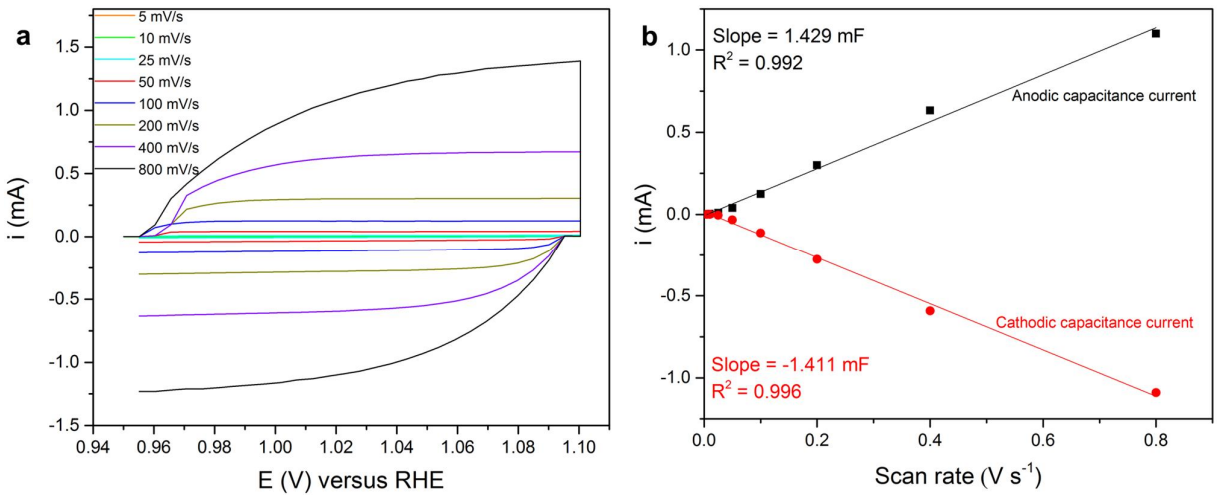

Figure S11. ***Double-layer capacitance measurements for g-Fe_2O_3/CNT catalyst from cyclic voltammetry in 1 M NaOH.*** **a,** Cyclic voltammograms of the g-Fe_2O_3/CNT electrode recorded in a non-faradaic region (0.95 V ~ 1.1V vs. RHE) at scan rates of 5, 10, 25, 50, 100, 200, 400, and 800 mV, respectively. The working electrode was held at each potential vertex for 10 s before the beginning the next sweep. All the current is assumed to be due to capacitive charging. **b,** The cathodic (red circle) and anodic (black square) capacitance currents measured at 1.02 V vs. RHE plotted as a function of scan rate. The double-layer capacitance of this system is calculated as the average of the absolute value of the slope of the linear fits to the data.

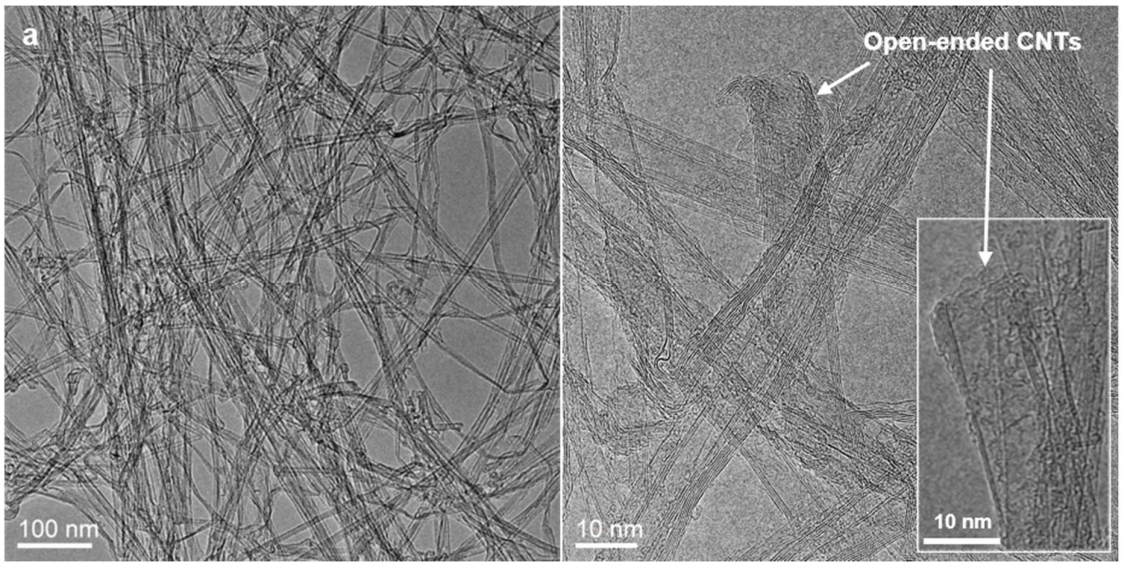

Figure S12. a, TEM and **b,** HRTEM images taken from the CEIN/CNT material electrochemically purified by 5 potential cycling between 1 and 1.6 V (vs RHE) in 0.5 M H_2SO_4 at a scan rate of 50 mV s^{-1}, indicating the removal of the iron impurities in CEINs from the sample. In image b, the CNTs with opened caps are visible.

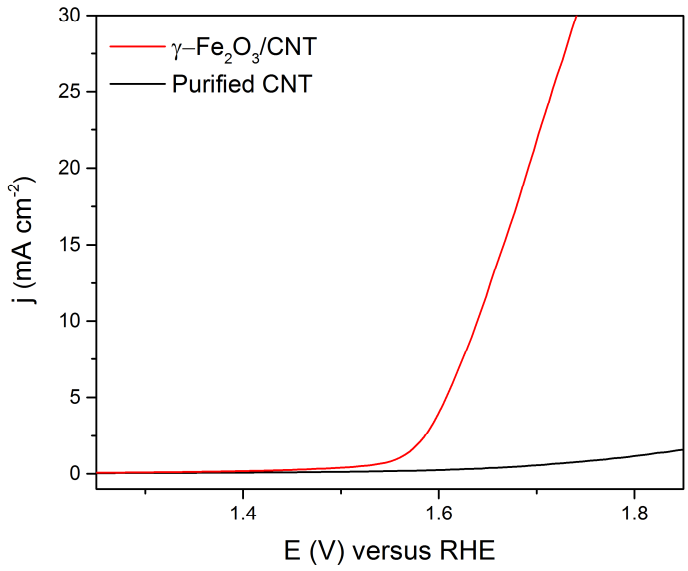

Figure S13. The polarization curves of the CEIN/CNT sample after stabilization of the OER current in alkaline solution (g-Fe_2O_3/CNT, red line) and after electrochemical purification in 0.5 M H_2SO_4 acidic solution (purified CNT, black line). The polarization curves were measured at a scan rate of 5 mV s^{-1} and a rotation of 1600 r.p.m in 0.1 M NaOH alkaline solution.

References

1. M. S. Dresselhaus, G. Dresselhaus and A. Jorio, *The Journal of Physical Chemistry C*, 2007, **111**, 17887-17893.
2. T. I. T. Okpalugo, P. Papakonstantinou, H. Murphy, J. McLaughlin and N. M. D. Brown, *Carbon*, 2005, **43**, 153-161.
3. C. Hontoria-Lucas, A. J. López-Peinado, J. d. D. López-González, M. L. Rojas-Cervantes and R. M. Martín-Aranda, *Carbon*, 1995, **33**, 1585-1592.
4. C. C. L. McCrory, S. Jung, J. C. Peters and T. F. Jaramillo, *J. Am. Chem. Soc.*, 2013, **135**, 16977-16987.
5. X. Lu, W.-L. Yim, B. H. R. Suryanto and C. Zhao, *J. Am. Chem. Soc.*, 2015, **137**, 2901-2907.
6. Y. Zhao, R. Nakamura, K. Kamiya, S. Nakanishi and K. Hashimoto, *Nat Commun*, 2013, **4**.
7. S. Dou, L. Tao, J. Huo, S. Wang and L. Dai, *Energy & Environmental Science*, 2016, DOI: 10.1039/C6EE00054A.
8. S. Mao, Z. Wen, T. Huang, Y. Hou and J. Chen, *Energy & Environmental Science*, 2014, **7**, 609-616.
9. T. Y. Ma, S. Dai, M. Jaroniec and S. Z. Qiao, *Angew. Chem. Int. Ed.*, 2014, **53**, 7281-7285.
10. M.-R. Gao, Y.-F. Xu, J. Jiang, Y.-R. Zheng and S.-H. Yu, *J. Am. Chem. Soc.*, 2012, **134**, 2930-2933.